RSC Advances

PAPER

View Article Online
View Journal | View Issue

Cite this: *RSC Adv.*, 2025, **15**, 46434

Exploring the antimicrobial properties of synthetic tetrahydro-2*H*-1,3,5-thiadiazine-2-thiones (THTTs) through *in vitro* and *in silico* antileishmanial and antibacterial studies

Rasool Khan, †*[a] Sumaya Raheem,†[a] Sobia Ahsan Halim,[b] Midrar Ullah,[c] Haleema Ali,[a] Imdad Ullah Khan,[i] Momin Khan,[d] Hanan A. Ogaly,[e] Mohammad Zubair,[fg] Mesaik M. Ahmed,[fg] Ajmal Khan*[bh] and Ahmed Al-Harrasi*[b]

Infectious diseases represent a significant health concern due to their high rates of morbidity and mortality. Despite significant advances in the understanding of the pathogenic infection, existing therapies to control those infections are still unsatisfactory. Herein, a total of 18 alkyl/aryl/aralkylamines or amino acids attached 1,3,5-thiadiazine-2-thiones (**4a–i**, **5a–g**, **6** and **7**) were synthesized *via* one pot domino synthesis and assessed their *in vitro* leishmanicidal and bactericidal potential. Their structures were confirmed through advanced spectroscopic techniques (^{1}H-NMR, ^{13}C-NMR, and HRMS analysis). The compounds inhibited promastigotes of *Leishmania tropica* with IC_{50} values ranging from 1.50 μg mL^{-1} to 72.04 μg mL^{-1}, where compounds **4d** (IC_{50} = 1.50 μg mL^{-1}) and **4f** (IC_{50} = 4.61 μg mL^{-1}) exhibited the most potent inhibition. The *in silico* analysis showed good binding potential of both the compounds for Pteridine reductase 1 (PTR1; a crucial enzyme in the life cycle of leishmania) and acceptable physicochemical and drug-like profile. In molecular dynamics simulations, **4d** showed greater potency for PTR1 with MM-PBSA estimated binding free energy of −18.72 ± 3.21 kcal mol^{-1}. Additionally, compound **7** demonstrates potent antibacterial activity against *Staphylococcus aureus* as compared to amoxicillin, while compounds **5g**, **4c**, **4d**, **4e**, **4f**, and **5b** showed significant inhibition of *Klebsiella pneumoniae*. These findings suggest that compound **7** exhibits selective antibacterial activity against *S. aureus*, whereas compound **4e** demonstrates broad-spectrum potential by targeting both Gram-negative and Gram-positive bacteria. The dose-dependent inhibition observed indicates the need for further structural optimization to enhance antibacterial potency. Additionally, compounds **4d** and **4f** displayed dual antileishmanial and antibacterial activities, making them promising candidates for further investigation and optimization to achieve clinically relevant efficacy.

Received 14th August 2025
Accepted 4th November 2025

DOI: 10.1039/d5ra05994a

rsc.li/rsc-advances

Introduction

Infectious diseases have always been one of the biggest threats to humans.[1] Leishmaniasis is a highly neglected disease that predominantly affects economically disadvantaged populations globally. It is a vector-borne infection, triggered by an obligatory intracellular protozoan of the genus *Leishmania*. Human infections with *Leishmania* parasites spread *via* the bite of female phlebotomine sand flies of the genera *Phlebotomus* in the old world and *Lutzomyia*, in the new world.[2] Around 2 million people are affected by leishmaniasis globally in developing countries, causing 70 000 deaths each year and approximately around 350 million people are deemed at the peril of contracting the infection. Moreover, leishmaniasis causes 2.4 million disability-adjusted life years (DALYs) worldwide due to its associated morbidity.[3]

For decades, sodium stibogluconate (Pentostam), and meglumine antimoniate (Glucantime) has been considered as

[a]*Institute of Chemical Sciences, University of Peshawar, Peshawar 25120, Pakistan. E-mail: rasoolkhan@uop.edu.pk*
[b]*Natural and Medical Sciences Research Center, University of Nizwa, PO Box 33, 616 Birkat Al Mauz, Nizwa, Oman. E-mail: ajmalkhan@unizwa.edu.om; aharrasi@unizwa.edu.om; Tel: +96825446502; +96825446328*
[c]*Institute of Bacha Khan Medical College, Khyber Medical University, Peshawar, Pakistan*
[d]*Department of Microbiology, Institute of Basic Medical Sciences, Khyber Medical University, Peshawar, Pakistan*
[e]*Chemistry Department, College of Science, King Khalid University, Abha 61421, Saudi Arabia*
[f]*Department of Medical Microbiology, Faculty of Medicine, University of Tabuk, Tabuk, 71491, Saudi Arabia*
[g]*Molecular Microbiology and Infectious Diseases Research Unit, University of Tabuk, Tabuk, 71491, Saudi Arabia*
[h]*Department of Chemical and Biological Engineering, College of Engineering, Korea University, Seoul 02841, Republic of Korea*
[i]*Department of Biotechnology, Abdul Wali Khan University, Mardan 23200, Pakistan*
† These authors contributed equally to this work and are first co-authors.

drugs of choice for management of leishmaniases, especially visceral leishmaniasis (VL) in immunocompetent patients. These drugs interfere with the parasite's glycolysis. However, their use has declined due to toxicity, treatment failures, and increasing parasite resistance, leading to the adoption of other therapies like amphotericin B and miltefosine.[4] Amphotericin B appears to be a better treatment option but can be poorly tolerated, and its lipid-based formulation has proven to be less toxic, yet the high cost renders it unusable. While miltefosine (an alternative for visceral leishmaniasis) and paromomycin (aminosidine; used with some success in cutaneous leishmaniasis) are registered clinical agents, however antimonial are often ineffective in immunocompromised individuals. Therefore, novel, improved, clinically safe and inexpensive antileishmanial drugs are need to be identified.[5]

Medicinal significance of tetrahydro-2*H*-1,3,5-thiadiazine-2-thiones (THTTs) as bioactive heterocycles has been recognized by numerous researchers, reporting their diverse biological activities, such as antimicrobial,[6–8] anti-atherosclerotic,[9] neuroprotective,[10] anticancer,[11–13] anti-inflammatory and analgesic agents.[14] The antimicrobial effects of these compounds are thought to result from dithiocarbamic acid and isothiocyanates formed upon *in vivo* hydrolysis of the THTT framework.[15] Additionally, several antibacterial drugs like amoxicillin,[16] ampicillin[17] chloramphenicol[8] and cefadroxil[18] (Fig. 1) have been conjugated to THTT skeleton to generate prodrugs. Meanwhile, compounds of this class has been approved as commercial fungicidal including sulbentine and milneb[19] (Fig. 1). Furthermore, THTTs have also shown promising antiprotozoal potential. While a few of 3-furfuryl-5-carboxyalkyl tetrahydro-(2*H*)-1,3,5-thiadiazine-2-thiones have inhibited all the developmental stages of *Leishmania amazonensis*.[20] Likewise, some glycine attached thiadiazinethione and their ester analogues have shown noteworthy *in vitro* antileishmanial activities.[21] This encouraged us to synthesize some new THTT derivatives with antileishmanial and antimicrobial potential.

This study represents an extension of our ongoing program focused on utilizing simple and readily available materials for the synthesis of diverse bioactive scaffolds.[14] The objectives of our research have been achieved through the synthesis of 18 THTT analogues and the evaluation of their *in vitro* leishmanicidal and bactericidal activities. Additionally molecular docking and molecular dynamics simulation of most potent analogue further unveiled the binding mechanism. The synthesized compounds are new to the best of our knowledge and have not been published for this activity before. Currently there are few compounds which show dual leishmanicidal and antibacterial potential. This study fills an important gap in knowledge by studying a novel group of alkyl/aryl/aralkylamine and amino acid-appended 1,3,5-thiadiazine-2-thione scaffolds, a class that remained largely overlooked for leishmanicidal and bactericidal activities.

Results

Chemistry

For the synthesis of THTTs, different methods have been reported including the use of isothiocyanate and solid phase organic synthesis.[9] However, the most used procedure proceeds *via* a dithiocarbamate salt intermediary. To synthesize target compounds, conventional one pot domino synthesis was carried out (Scheme 1).[14] Different alkyl/cycloalkyl/aralkylamines or amino acids and KOH in aqueous media were reacted with CS_2. The mixture was continuously stirred for 4 hours to afford intermediate **2**. Formaldehyde was poured into it portion wise to bear intermediate **3**, which was filtered, and the solution was transferred slowly to a stirred solution of different alkyl/cycloalkyl/aralkylamines or amino acids in slightly basic (pH 7.8) phosphate buffer media. This enabled the formation of diversified THTTs scaffolds (**4a–i**, **5a–g**) and structures were deduced by spectroscopic characterizations.

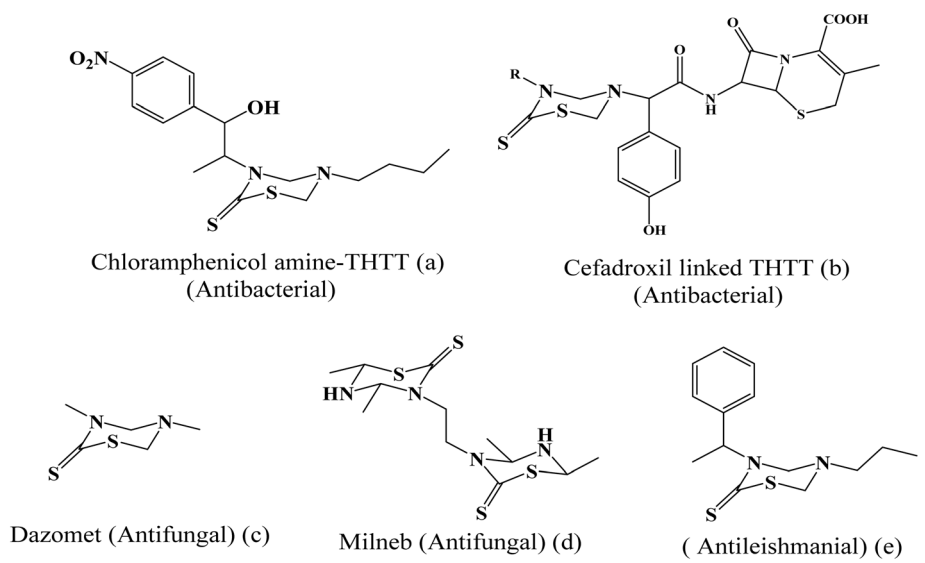

Fig. 1 Bioactive compounds (a)–(e) comprising of 1,3,5-thiadiazine-2-thione (THTT) skeleton.

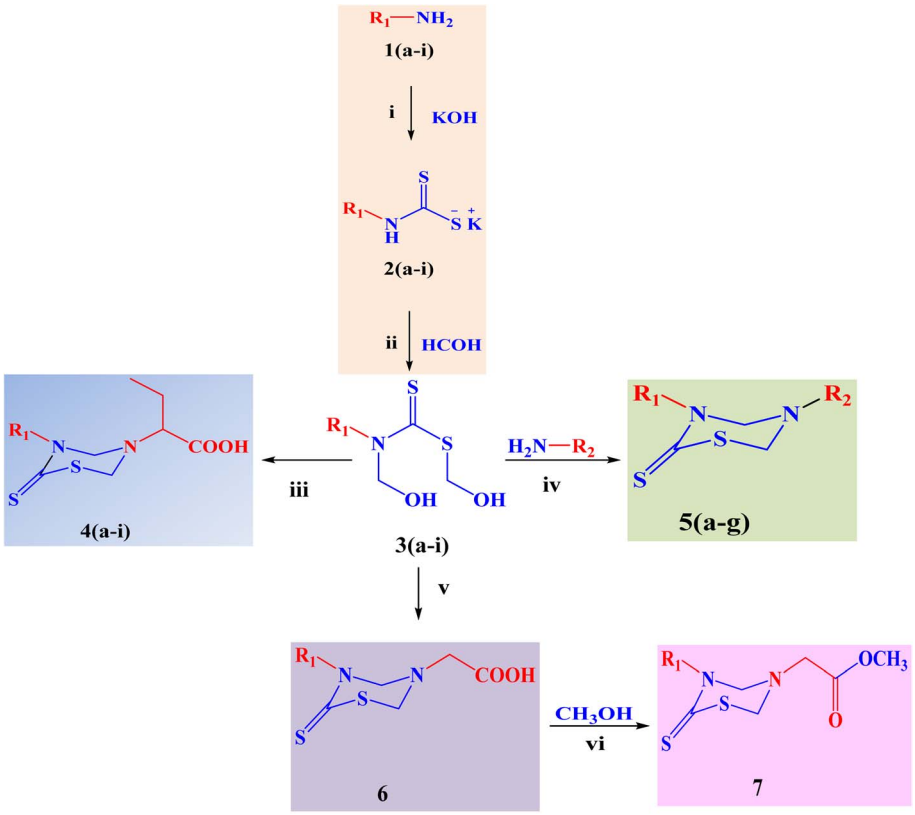

4a = R_1 = Methyl
4b = R_1 = Ethyl
4c = R_1 = Propyl
4d = R_1 = Octyl
4e = R_1 = Dodecyl
4f = R_1 = Benzyl
4g = R_1 = Furfuryl
4h = R_1 = Phenyl
4i = R_1 = Cyclohexyl

5a = R_1 = $CH_2CH_2CHCOOH$, R_2 = Benzyl
5b= R_1 = $CH_2CH_2CHCOOH$, R_2 =furfuryl
5c = R_1 = Phenyl, R_2 =furfuryl
5d = R_1 = HO-CH_2-CH_2-, R_2 = $HOOCCH_2$-
5e = R_1 = Methyl, R_2 = Pyridine-yl
5f = R_1 = $CH_2CH_2CHCOOH$, R_2 = Cyclohexyl
5g = R_1 = Isopropyl R_2 = Isopropyl
6 = R_1 = $CH_3CH_2CH_2CH_2$-
7 = R_1 = $CH_3CH_2CH_2CH_2$-

Scheme 1 Synthetic scheme of tetrahydro-2*H*-1,3,5-thiadiazine-thiones series A (**4a–i**), B (**5a–g**), **6** and **7**. Reaction conditions: (i) primary amines (**4a–i**) (20 mmol), water (25 mL), CS_2 (2 equiv., 2.4 mL), KOH (20%, 1.120 mg), temperature 25 °C, time 4 h; (ii) HCHO (2 equiv., 35%), temperature 25 °C, time 1 h; (iii–v) primary amines (1 equiv., (20 mmol)), phosphate buffer pH 7.8, 20 mL, temperature 25 °C, time 1 h; (vi) THTT 6 (1 mmol), $SOCl_2$ (1.5 equiv.), CH_3OH (10 mL), temperature 0–4 °C, time 30 minutes.

Infrared (IR) spectroscopy showed carbonyl (C=O) and thiocarbonyl (C=S) absorptions in the range of 1761–1690 cm^{-1} and 1511–1460 cm^{-1}, respectively. Absorption peaks at 3450–3300 cm^{-1} corresponds to carboxylic acid O–H. In the ^1H NMR spectra, two separate signals were observed for C-4 and C-6 methylene protons at around δ 5.26 to δ 3.65 ppm. However, for some molecules ring methylene protons were shown as either doublets or multiplets. Likewise, in compounds **4b–d**, methylene protons at N-3 looked as duplicated multiplets. The ^{13}C NMR spectra displayed signals for C-4, and C-6 around δ 69.7, and δ 59.7 ppm, respectively. The thiocarbonyl functional group was seen at δ 190–193 ppm and COOH carbon was seen at δ 170–174 ppm.

Biological activities

Antileishmanial activity. The leishmanicidal activities of compounds are summarized in Table 1. The assessment was done at 100, 50 and 25 μg mL^{-1} concentrations, using a preformed culture of *L. tropica*. Parasite viability was estimated using 3-(4,5-dimethylthiazol-2 yl)-2,5-diphenyl tetrazolium bromide (MTT) assay in which the amount of formazan formed is directly related to the number of metabolically active cells. We found the concentrations that reduced the cell growth of promastigotes by 50% (IC_{50}) for the THTTs scaffolds and standard drug (amphotericin B, one of the most active leishmanicidal agent). Compounds **4a–i**, **5a–g**, **6** and 7 showed varying levels of leishmanicidal activities with IC_{50} ranging from 1.5 to 72 μg

Table 1 IC_{50} values of the compounds against *Leishmania tropica*[a]

Compounds	IC_{50} (μg mL^{-1})	Compounds	IC_{50} (μg mL^{-1})
4a	12.50	**5a**	20.40
4b	28.86	**5b**	72.04
4c	23.42	**5c**	10.38
4d	1.50	**5d**	14.69
4e	12.2	**5e**	24.81
4f	4.61	**5f**	15.28
4g	55.95	**5g**	25.06
4h	13.0	**4i**	20.5
6	10.00	**7**	50.32

[a] Standard drug: amphotericin B (IC_{50} = 0.58 μg mL^{-1}).

mL^{-1}. The highest inhibitory potential was shown by compound **4d** (IC_{50} = 1.5 μg mL^{-1}) relative to amphotericin B, followed by **4f** (IC_{50} = 4.61 μg mL^{-1}). Compounds **4a**, **4e**, **4h**, **5c**, **5d**, **5f** and **6** demonstrated significant inhibitory activities with IC_{50s} ranges from 10 to 20 μg mL^{-1}. While the rest of the compounds showed minimum to moderate activity (<20 μg mL^{-1}).

Antibacterial activity. The bactericidal prospect of the compounds **4a–i**, **5a–g**, **6** and **7** was measured against *Staphylococcus aureus* and *Klebsiella pneumoniae* using agar well diffusion method at different concentrations (4000 μg mL^{-1}, 2000 μg mL^{-1}, and 1000 μg mL^{-1}). The results are presented as the zones of inhibition (in mm) in Table 2. Out of tested 18 molecules, compound **7** showed activity against Gram-negative *S. aureus* followed by **5d**, **5e**, **4e**, **5a**, **5c**, and **4c** at 4000 μg mL^{-1}. The inhibitory potential of compound **7** (zone of inhibition = 31 mm) was higher than that of amoxicillin (standard drug) which displayed zone of inhibition of 30 mm at 4000 μg mL^{-1}. While compounds **5d** and **5e** showed zone of inhibition of 22 mm each at 4000 μg mL^{-1}. At 4000 μg mL^{-1}, all the compounds showed inhibitory potential for *K. pneumoniae* where **5g** showed highest inhibition with 26 mm of zone of inhibition relative to amoxicillin (32 mm), followed by **4c**, **4d**, **4e**, **4f**, and **5b**. However, at 2000 μg mL^{-1} and 1000 μg mL^{-1}, compounds did not show significant inhibition. These results indicate that compound **7** could be a selective antibacterial agent for *S. aureus* while compound **4e** can target both Gram negative and Gram positive bacteria. The compounds showed dose dependent inhibition, therefore further structural optimization of molecules is needed to enhance their antibacterial efficacy. Moreover, we observed that compounds **4d** and **4f** possess dual antileishmanial and antibacterial activities, therefore these two molecules are of interest for further studies and should be further optimized to improve their potency to clinically relevant levels.

Structure–activity relationship. Increasing the lipophilicity of drug scaffolds enhances their ability to penetrate biomembrane, as a result rising their infusion toward cell membranes of microbes. Optimum activities had been revealed by compounds carrying lipophilic moiety at the N-3 position and hydrophilic ones at the N-5 position 25. Both the activities mainly depended upon the type of the substituents at position N-3 and N-5 of the main thiadiazine ring. Among the series, compound **4d** and **4f** with nonpolar octyl and benzyl groups at N-3 showed highest leishmanicidal activity, exhibiting IC_{50} values 1.50 μg mL^{-1} and 4 μg mL^{-1}, respectively. It is pertinent to compare the antileishmanial activity of compound **6**, which

Table 2 Antibacterial potential of compounds against *S. aureus* and *K. pneumoniae* at three different concentrations

		Zone of inhibition diameter in mm					
		Staphylococcus aureus			*Klebsiella pneumoniae*		
S. no.	Compounds	4000 μg mL^{-1}	2000 μg mL^{-1}	1000 μg mL^{-1}	4000 μg mL^{-1}	2000 μg mL^{-1}	1000 μg mL^{-1}
1	**4a**	0	0	0	20	16	10
2	**4b**	0	0	0	19	12	8
3	**4c**	12	0	0	24	17	12
4	**4d**	0	0	0	23	16	10
5	**4e**	19	14	10	22	18	14
6	**4f**	0	0	0	22	18	12
7	**4g**	0	0	0	21	16	12
8	**4h**	0	0	0	10	0	0
9	**4i**	0	0	0	9	0	0
10	**5a**	17	14	6	13	0	0
11	**5b**	0	0	0	22	14	10
12	**5c**	17	12	10	14	10	0
13	**5d**	22	18	16	20	16	10
14	**5e**	22	17	12	21	15	10
15	**5f**	0	0	0	15	10	0
16	**5g**	0	0	0	26	18	12
17	**6**	0	0	0	20	16	10
18	**7**	31	22	18	17	12	6
19	DMSO	0	—	—	—	0	—
20	Amoxicillin (100 μg mL^{-1})	30	—	—	32	—	—

displayed a very noteworthy level of activity (IC_{50} = 10.26 μg mL^{-1}) with its methyl ester derivative **7** displaying IC_{50} of 50.32 μg mL^{-1}. This reduction did not astonish us as esters have been identified to get active under biological setting *via* changing back into carboxylic acids by esterases, thus follow prodrug criterion.[21] Decreasing polarity in compound **7** has increased its bactericidal potential relative to compound **6** suggesting its enhanced bio-membrane permeability.

Molecular docking and ADMET analysis of 4d and 4f. Pteridine reductase 1 (PTR1) was selected as the target to dock our most potent compounds because this enzyme has prime importance in the parasite's folate and biopterin metabolic pathways, parasite survival and virulence. PTR1 plays a crucial role in the reduction of both oxidized biopterins and folates, compensating for the inhibition of dihydrofolate reductase–thymidylate synthase (DHFR-TS) and thereby conferring resistance to antifolate drugs. It contributes to the failure of conventional therapies, such as methotrexate, against these protozoans. PTR1 gene knockout studies in leishmania and *Trypanosoma brucei* have demonstrated that this enzyme is essential for parasite survival. Inhibiting PTR1 is therefore a validated strategy for antileishmanial drug discovery, and several studies have highlighted it as a promising therapeutic target. Therefore, in the current study, we focused on targeting PTR1 using molecular docking strategy. Two compounds, **4d** and **4f** showed excellent leishmanicidal potential, therefore these molecules were docked into the binding cavity of PTR1 enzyme, where the molecules showed excellent complementarity with the active site. Both the molecules demonstrated strong binding potential for PTR1 by binding through several residues with highly negative docking scores. Compound **4d** formed hydrogen bonds with Gly225, Ser227, Ser111 and Lys198. The butanoic acid of **4d** interacted with Gly225 and Ser227 at 1.97 Å and 3.17 Å, respectively. While the thiadiazinane–thione moiety of **4d** accepted hydrogen bonds with Ser111 (3.89 Å) and Lys198 (3.27 Å). Compound **4d** produced −6.97 kcal mol^{-1} docking score in the PTR1. Similarly, the butanoic acid of **4f** interacted with Ser227 at 2.47 Å, while its thiadiazinane–thione moiety accepted hydrogen bonds from Lys198 at 2.33 Å. Moreover, the phenyl ring of **4f** exhibited hydrophobic interaction (π-cation) with Arg17 at 3.23 Å. **4f** exhibited a docking score of −6.10 kcal mol^{-1} with PTR1, reflecting slightly higher binding affinity of **4d** for PTR1 than **4f** (as identified *in vitro*). The 3D- and 2D-interactions of compounds are given in Fig. 2.

When the docking results of **4d** and **4f** were compared with the standard inhibitor (2∼{*R*}fi)-2-[3,4-bis(oxidanyl)phenyl]-6-oxidanyl-2,3-dihydrochromen-4-one, co-crystalized in 5L42, we observed that this ligand only mediates a hydrophobic interaction with the surrounding residue and forms a hydrogen bond with co-enzyme and exhibit a docking score of −5.88 kcal mol^{-1}. It predicts that our compounds have higher binding potential than the standard inhibitor used in docking analysis.

In ADME analysis, both compounds **4d** and **4f** exhibit favorable physicochemical and pharmacokinetic profiles with high gastrointestinal absorption, balanced water solubility and lipophilicity, no blood–brain barrier permeability, no P-glycoprotein substrate-likeness and no major drug-likeness violations. Compound **4d** has a higher molecular weight, greater lipophilicity, and more rotatable bonds, indicating its higher flexibility than **4f**. In contrast, **4f** demonstrates better balance in aromaticity (C_{sp^3} = 0.43), solubility, and synthetic accessibility, fulfilling lead-likeness criteria. Overall, these compounds emerge as the more promising lead candidate due to their favorable drug-likeness, solubility, and ease of synthesis, making it a suitable scaffold for further optimization. The results are summarized in Table 3.

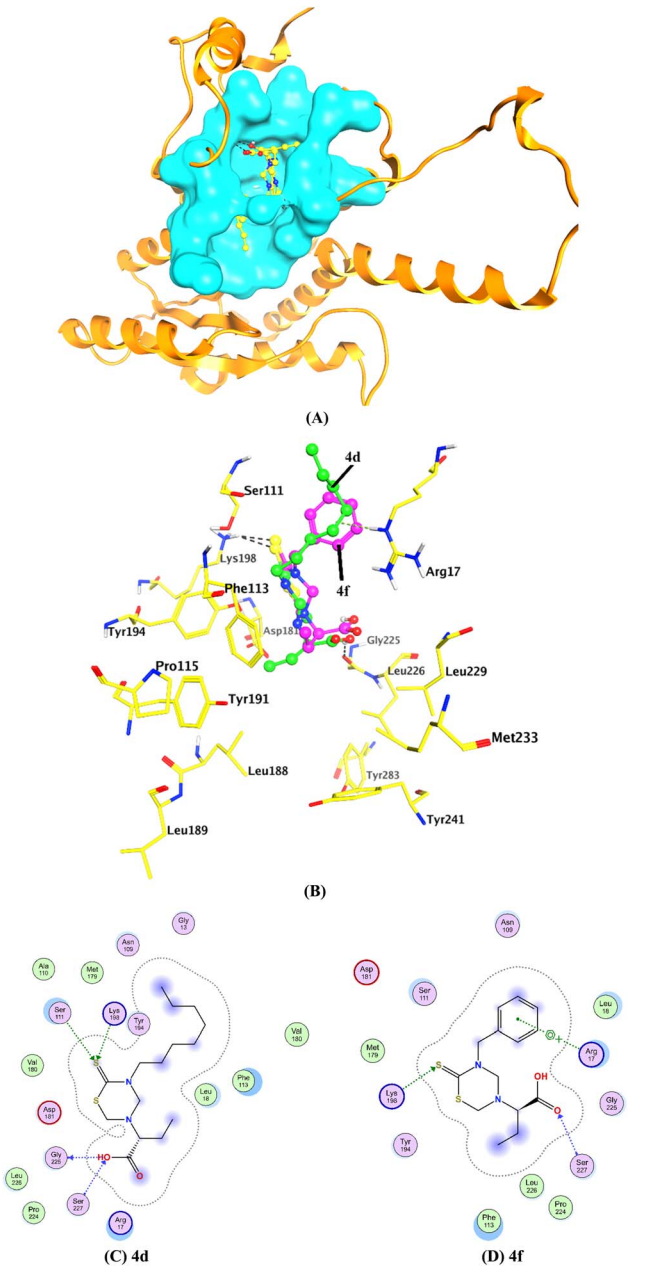

Fig. 2 (A) The binding modes of **4d** and **4f** (yellow ball and sticks) are shown in PTR1 enzyme (orange ribbon). The active site is shown in surface model. (B). The interactions of compounds are shown with the active site residues of PTR1. Hydrogen bonds are shown in black dashed lines. (C and D) 2D-interactions of **4d** and **4f** are shown.

Molecular dynamics simulation. Compound **4d** was subjected to molecular dynamic simulations to study the dynamic behavior of **4d**-PTR1 complex and their interaction along with standard inhibitor complex with PTR1 (STD). STD showed initially low RMSD than **4d**-complex, however, after 140 ns, the RMSD of **4d** suddenly decreased (9.8 Å) than that of STD (10.8 Å)

Table 3 ADME results of compounds **4d** and **4f**

	Compounds	
	4d	**4f**
Physicochemical properties		
Formula	$C_{15}H_{28}N_2O_2S_2$	$C_{14}H_{18}N_2O_2S_2$
Molecular weight	332.53 g mol^{-1}	310.43 g mol^{-1}
Num. heavy atoms	21	20
Num. arom. heavy atoms	0	6
Fraction C_{sp^3}	0.87	0.43
Num. rotatable bonds	10	5
Num. H-bond acceptors	3	3
Num. H-bond donors	1	1
Molar refractivity	102.88	93.72
TPSA	101.17 Å^2	101.17 Å^2
Lipophilicity (log $P_{o/w}$)	3.00	1.69
Water solubility (log S)	−3.09 (soluble)	−2.29 (soluble)
Pharmacokinetics		
GI absorption	High	High
BBB permeant	No	No
P-gp substrate	No	No
CYP1A2 inhibitor	No	No
CYP2C19 inhibitor	Yes	No
CYP2C9 inhibitor	No	No
CYP2D6 inhibitor	No	No
CYP3A4 inhibitor	No	No
log K_p (skin permeation)	−6.25 cm s^{-1}	−7.48 cm s^{-1}
Druglikeness		
Lipinski	Yes; 0 violation	Yes; 0 violation
Ghose	Yes	Yes
Veber	Yes	Yes
Egan	Yes	Yes
Muegge	Yes	Yes
Bioavailability score	0.55	0.55
Medicinal chemistry		
PAINS	0 alert	0 alert
Brenk	1 alert: thiocarbonyl_group	1 alert: thiocarbonyl_group
Leadlikeness	No; 1 violation: rotors >7	Yes
Synthetic accessibility	4.05	3.40
Boiled egg	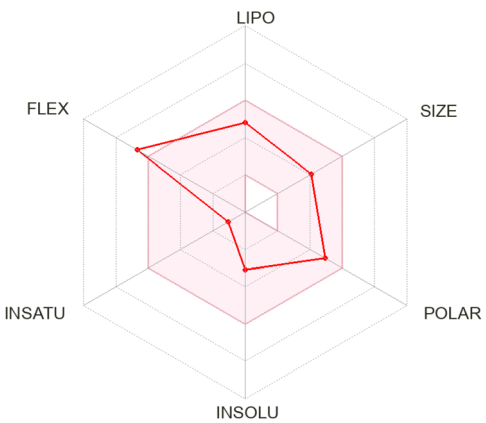	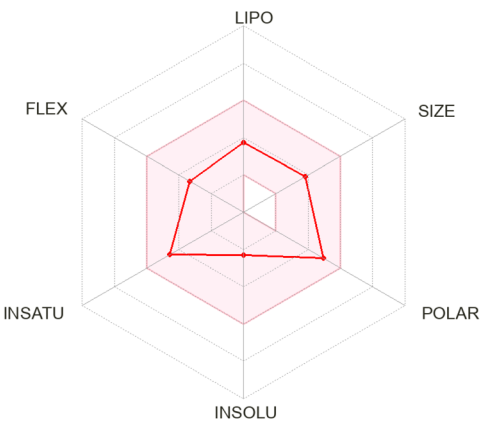

indicating that **4d** effectively stabilize the protein as compared to STD. The RMSD graph is shown in Fig. 3A. The residual fluctuation gives significant information about protein's conformational changes pre-/post-ligand binding. This can be analyzed by root mean square residual fluctuation (RMSF). RMSF graph shows large fluctuation in the residue 40, 80, 120, 160, 180 and 240–281 in the STD-complex, while the **4d** showed similar pattern of fluctuation but peaks are lower than STD except residue 40, 80, and 200. Overall, small fluctuations in the **4d**-complex shows that the complex is stabilized well after binding of **4d**, suggesting more potency of **4d** than STD (Fig. 3B).

A more detailed analysis for residual fluctuations and the dynamics of protein before and after ligand binding was done by 2d-RMSD. Different color contours represent different conformations, and more color contours indicate more conformations. Fig. 3C shows large number of color contours in STD-complex indicating large conformational changes in STD bound-complex. However, **4d**-complex showed an opposite effect (less number of color contour after binding). The 2d-RMSD correlates with RMSF and RMSD and proves **4d** stabilizes the complex.

The dynamic features of PTR1 after ligand binding were further explored by dynamical cross correlation matrix (DCCM) analysis (Fig. 4A). In DCCM, a positive correlation coefficient (colored red/pink) indicates positively correlated movement, where atoms or residues move in the same direction, while a negative coefficient (colored blue) signifies anticorrelated movement, meaning they move in opposite directions. In STD-complex, dominant correlated movement is shown by residues 1–100, while residues 100–150 and 250–281 shows dominated anticorrelated movement, whereas residues 150–250 shows no linear correlation. In **4d**-complex, mostly no correlation was observed, however the negative correlations were dominated over positive correlation, but pattern of correlation was unlike

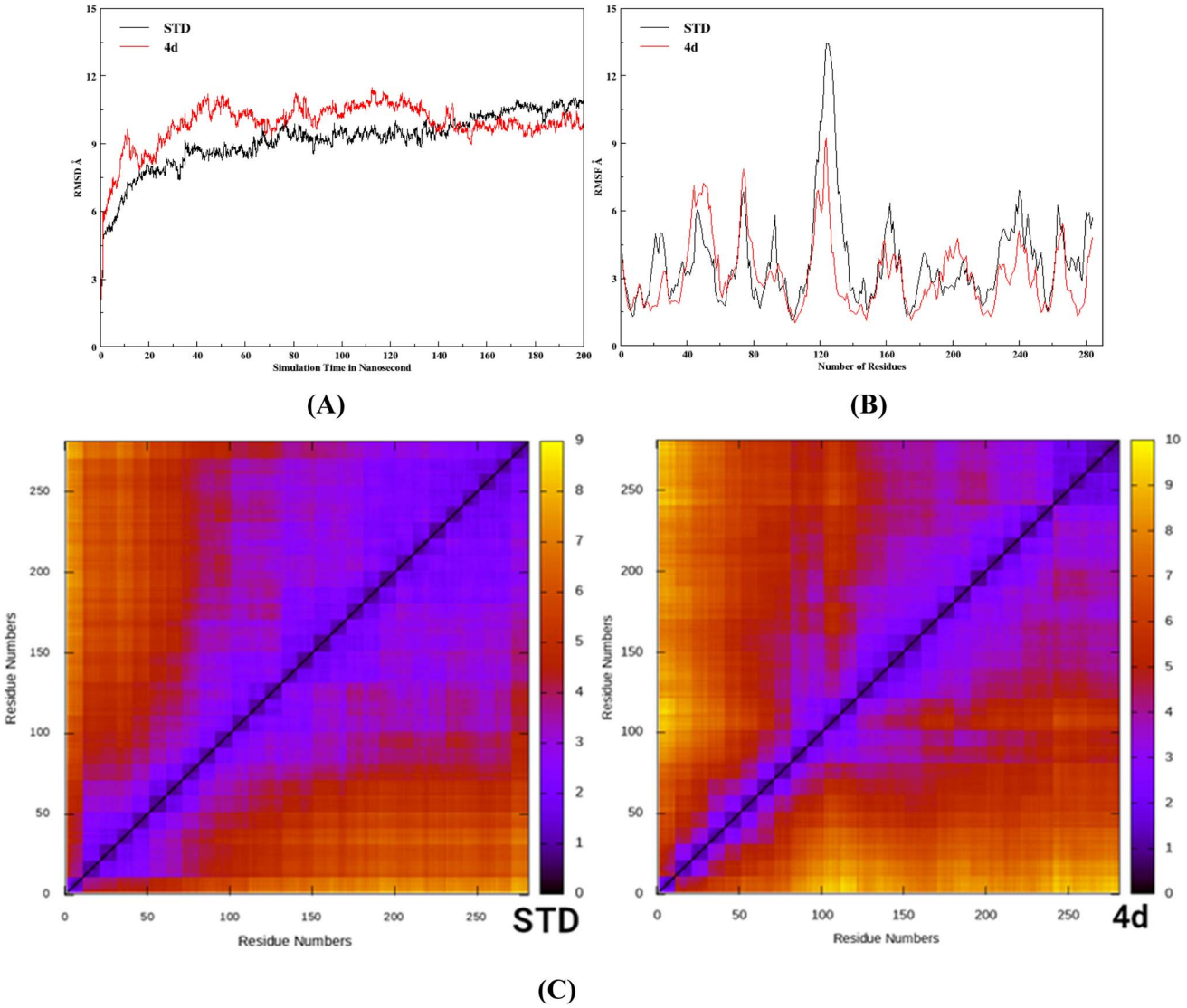

Fig. 3 (A) RMSD (B) RMSF and (C) 2d-RMSD graphs of STD and **4d**.

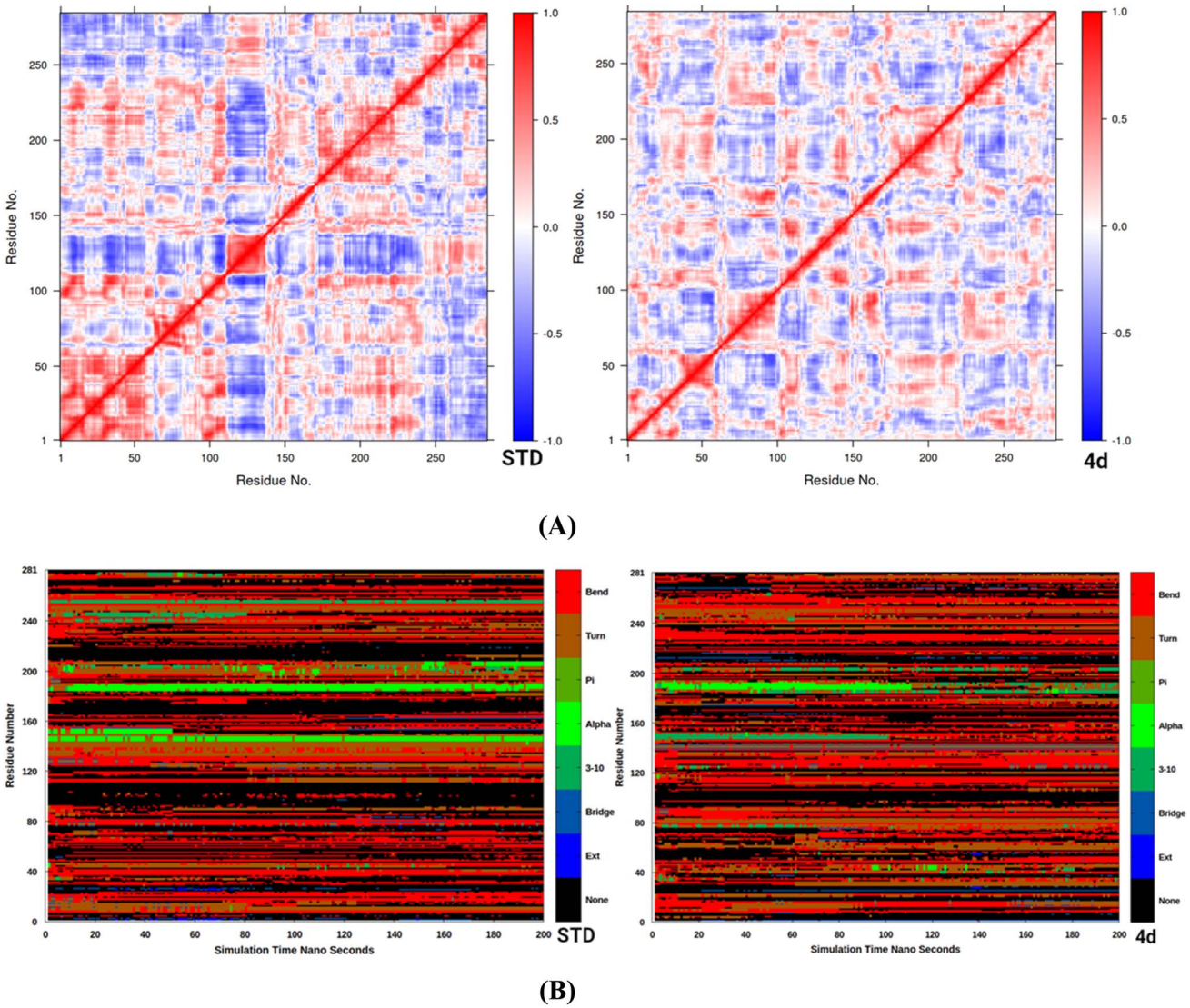

Fig. 4 DCCM (A) and DSSP (B) plots of STD and **4d**-complex.

STD. The results indicate that STD has closed conformation while **4d** has open conformation.

Furthermore, the secondary structures of PTR1 were examined by DSSP (Define Secondary Structure of Proteins), which has significant information of conformational variation in protein with time (Fig. 4B). DSSP plot shows how the secondary structure elements (SSEs) of each residue (*y*-axis) evolve over simulation time (*x*-axis). STD-complex shows frequent red/orange regions, suggesting dominance of bends and turns, indicating flexible loops. While α-helix (green patches) appear mainly between residues 150–180 and 190–210, showing stable helices. Scattered black regions indicate local unfolding or dynamic motion. In **4d**-complex, the pattern is broadly similar, however α-helices (green) in the 150–210 region appear more continuous, implying increased helical stability. Slight reduction in black regions, indicating fewer disordered parts. Some β-bridges (blue) persist longer in specific regions (perhaps stabilizing β-structure). The **4d** system seems to enhance secondary structure stability, especially α-helices, compared to the STD system. This stabilization could be due to ligand binding reducing flexibility or lower conformational entropy in complex form.

Furthermore, radius of gyration (R_g) was computed to explore the structural flexibility of the protein in STD-/**4d**-complexes (Fig. 5A). Secondary structure evolution and R_g analyses collectively provide insights into the conformational stability of the protein in STD-/**4d** complexes. The DSSP plots revealed that both systems predominantly contain bends and turns, reflecting the inherent flexibility of the protein. However, the **4d**-complex exhibited more persistent α-helical regions, particularly between residues 150–210, compared to the STD system, indicating enhanced helical stability and a tendency toward local structural order upon ligand binding. In contrast, the STD system showed intermittent loss of secondary structure, suggesting greater conformational fluctuations. The R_g profiles further supported these observations. The **4d**-complex

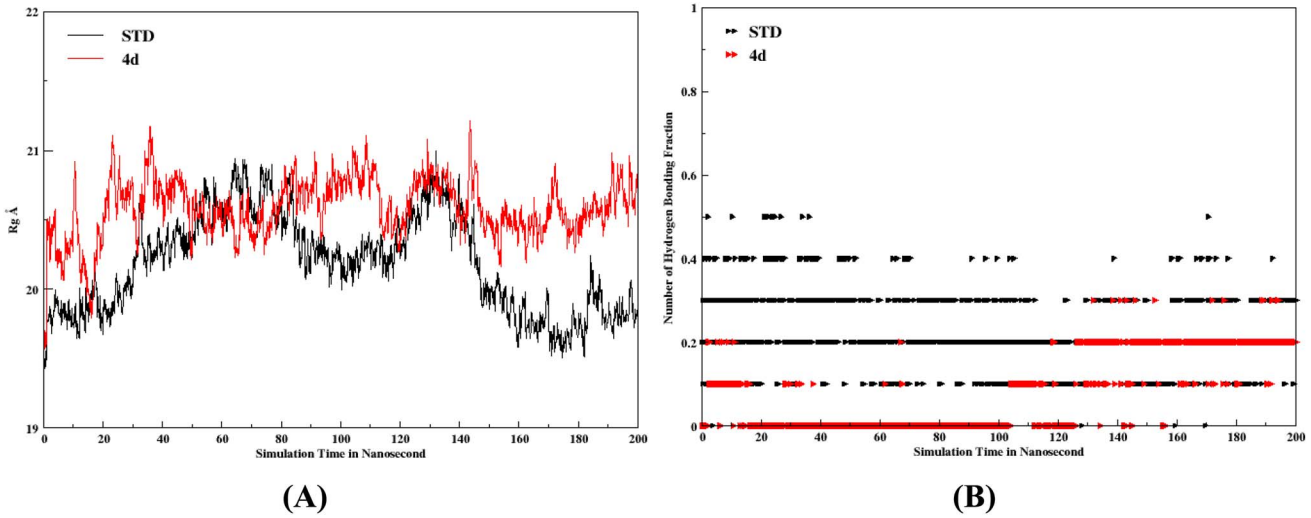

Fig. 5 R_g (A) and HBF (B) plots of STD and **4d**-complex.

maintained a slightly higher average R_g (~21 Å) compared to the STD-complex (~20 Å), implying a less compact but dynamically stable conformation. This expansion could be attributed to ligand-induced conformational rearrangements or domain movements that accommodate binding interactions. Meanwhile, the STD-complex exhibited a gradual decrease in R_g toward the end of the simulation, suggesting a return to a more compact, native-like state. These results suggest that the **4d** promotes secondary structural stabilization (particularly α-helices) while allowing moderate global expansion and flexibility, which may facilitate functional conformational dynamics or binding-induced adaptations within the protein.

Hydrogen Bonding Fraction (HBF, Fig. 5B) shows polar interaction of ligand and protein, it provides important information about hydrogen bonding fluctuations during simulation. HBF of STD has maximum 0.5 and consistent 0.2. In **4d**-complex, the maximum HBF is 0.3 with no consistent HBF. It suggests that polar interaction of STD is stronger than **4d**. The hydrogen bonding analysis revealed that the STD system formed a higher number and stronger hydrogen bonds throughout the simulation, while the **4d** system displayed fewer but more uniformly distributed hydrogen bonding interactions. The reduction in hydrogen bonding within the **4d** complex likely arises from ligand occupancy or local conformational adjustments that disrupt existing hydrogen-bond networks. However, the persistence of moderate hydrogen bond fractions suggests maintained dynamic stability despite the reduced bonding count. Overall, DSSP, R_g and HBF analysis indicate that ligand binding in the **4d**-complex promotes secondary structural stabilization (especially α-helices), accompanied by moderate expansion and flexible dynamics. This conformational adaptability likely facilitates the accommodation of the ligand while preserving global structural integrity, whereas the STD system remains more compact and hydrogen-bond stabilized, characteristic of a native-like stable protein conformation.

MM-PBSA calculation. For the detailed interactions of the ligand protein, we calculated polar and non-polar energies *via* MM-PBSA method. The total energy of STD is −18.72 ± 3.21 kcal mol^{-1}, while **4d** is −21.37 ± 3.04 kcal mol^{-1} (Table 4). The total energy is due to Van der Waal, electrostatic, polar solvation and solvent accessible surface area (SASA) energies. STD have −43.75 ± 2.77 kcal per mol VDW energy, −14.71 ± 2.81 kcal mol^{-1} of electrostatic energy, the polar component of solvation-free energy (GB) is 43.358 ± 2.62 and the non-polar component of the solvation energy (SASA) is −03.622 ± 0.17. The **4d** has VDW energy is −31.840 ± 4.75, electrostatic energy is −16.160 ± 2.79, the polar component of solvation-free energy GB is 30.044 ± 5.06 and the non-polar component of the solvation energy SASA is −03.408 ± 0.29. The result from energy all components of energy of STD is larger than **4d** except total energy which large repulsive energy of polar solvation-free energy (GB), which will support all *in silico* analysis, also correlates with the *in vitro* result comp_15 good inhibitor for *L. tropica*.

Table 4 Binding free energy calculation of the selected inhibitor compounds against *L. tropica*[a]

	MM-PBSA calculations (all units kcal mol^{-1}) differences (complex–receptor–ligand)				
Compounds	ΔE_{VDW}	ΔE_{EEL}	ΔE_{GB}	ΔE_{surf}	ΔG_{total}
STD	−43.747 ± 2.77	−14.708 ± 2.81	43.358 ± 2.62	−03.622 ± 0.17	−18.719 ± 3.21
4d	−31.840 ± 4.75	−16.160 ± 2.79	30.044 ± 5.06	−03.408 ± 0.29	−21.368 ± 3.04

[a] ΔE_{VDW} = van der Waals free energy, ΔE_{EL} = electrostatic free energy, ΔE_{GB} = the polar component of solvation-free energy, ΔE_{surf} = the non-polar component of the solvation energy, ΔG_{total} = total binding free energy.

Discussion

The data obtained from spectroscopic analysis of the synthesized THTT scaffolds are according to the previous reports.[15] IR analysis showed typical absorptions for functional groups like carbonyl (C=O) and thiocarbonyl (C=S) in the ranges 1761–1691 cm^{-1} and 1512–1461 cm^{-1}, respectively, which is similar to the literature data for similar reported heterocycles. The O–H stretch at 3450–3300 cm^{-1} is broad and confirms carboxylic acid functional group. In the ^{1}H NMR spectra, methylene protons at C-4 and C-6 displayed distinct chemical shifts around δ 5.26 to δ 3.65 ppm, however, for those molecules having stereocenter, the phenomena of diastereotopicity were observed as the ring methylene protons were shown as either doublets or multiplets are in line with the behavior reported for such ring systems.[22] Likewise, in compounds **4b–d**, methylene protons at N-3 looked as duplicated multiplets due to the chiral substituent on N-5. Similarly, ^{13}C NMR spectra further confirmed ring closure by displaying signals for C-4, and C-6 around δ 69.7, and δ 59.7 ppm, respectively. The thiocarbonyl functional group was seen in the range δ 190–193 ppm, as expected, while signals in the range δ 170–174 ppm appeared due to COOH carbon.

Utilizing the carboxylic part of the synthesized THTTs, we tried to exploit the possibility of esterification reaction for further derivatization of the THTT derivatives at N-5 (Scheme 1). The synthesized compounds were esterified with chlorinating agent thionyl chloride and alcohol which acted both as reagent and reaction medium. Initially 2-aminobutanoic acid was used as carboxylic acid moiety but none of the employed THTTs rendered any esterification product. Neither increased amount of thionyl chloride nor longer reaction times worked. However, glycine appended THTT (**6**) afforded the esterified product. Initially, the obtained products were gummy but with excess alcohol to dilute the reaction mixture and decrease the decomposed products of thiadiazinethione core with acidic thionyl chloride rendered the final product as colorless crystals.

The WHO predicts that antimicrobial infections may cause 10 million deaths annually by 2050, a consequence of both rising microbial drug resistance and the limited rate of new antimicrobial discovery.[23]

The thiadiazinethione scaffold has been extensively explored for various therapeutic applications, with its biological activity reported to occur in protic media through the formation of dithiocarbamic acid and isothiocyanates *via* hydrolysis of the thiadiazinethione moiety.[24] The THTT derivatives reported in this study are expected to decompose into N3-alkylisothiocyanates, such as benzyl isothiocyanates (BITCs) and methyl isothiocyanates (MITCs), which are well-documented for their antimicrobial properties. Additionally, potential interactions of the amino acids or amines appended at the 5-position of the THTT heteroring with other molecular targets cannot be excluded, which may further contribute to the enhanced biocidal activity observed for these scaffolds.[25,26]

Infections due to *S. aureus* continue to cause a major impact on human health, being a usual cause of respiratory infections, derma infections, and food poisoning.[27] *S. aureus* is considered one of the main pathogen for the leading cause of death associated with the emergence of methicillin-resistant *S. aureus*.[28] The bactericidal prospect of the synthesized heteroring THTTs was evaluated *via* well diffusion method. Among the tested series, compound **4e**, **5a**, **5c**, **5d**, **5e** and **7** showed significant inhibitory activities against the *S. aureus* (Table 2). Compound **7** showed most potent inhibition (with zone of inhibition = 31 mm at 4000 μg mL^{-1}, ZOI = 22 mm and 18 mm at 2000 μg mL^{-1} and 1000 μg mL^{-1}, respectively) surpassing the standard drug (amoxicillin, ZOI = 30 mm at 100 μg mL^{-1}) followed by **5d** and **5e**. This suggests potent bactericidal potential of compound **7**. Conversely, many compounds from the 4-series showed no noticeable potential against *S. aureus*, demonstrating their poor membrane permeability as most of them contain highly polar carboxylic acid moiety.

Klebsiella pneumoniae is an important Gram-negative bacterium and is usually linked with urinary tract infections and pneumonia.[29] Keeping in view the paucity of new drugs, we assessed our synthetic analogues against *K. pneumoniae*. All our synthesized heteroring THTTs were found highly significant at all three concentrations. Compound **5g** showed highest potency (26 mm, 18 mm and 12 mm at 4000 μg mL^{-1}, 2000 μg mL^{-1} and 1000 μg mL^{-1}, respectively) among the tested hits. Moreover, compounds **5g**, **5d**, **4c**, **4e** and **5e** also revealed strong inhibition of *K. pneumoniae*. Most potent compound against *L. tropica* was **4d** (IC_{50} = 1.50 μg mL^{-1}). This activity is closest to amphotericin B, suggesting that **4d** could be a promising lead after structural optimization. While several compounds including **4f** (IC_{50} = 4.61 μg mL^{-1}), **6** (IC_{50} = 10.00 μg mL^{-1}), and **5c** (IC_{50} = 10.38 μg mL^{-1}) showed moderate inhibitory activities. In conclusion, this study provides a proof-of-concept for the development of lead scaffolds with dual antileishmanial and antibacterial activity. While primarily exploratory, the findings demonstrate the therapeutic potential of these compounds and lay the groundwork for future optimization through structural modifications and SAR studies to enhance potency and achieve clinically relevant efficacy.

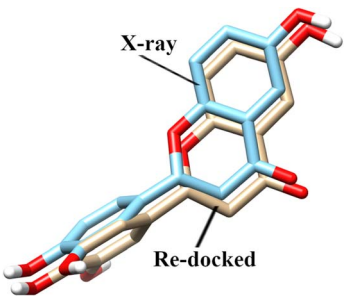

Fig. 6 The re-docked conformation (gold) is superimposed on the X-ray conformation (blue) of co-crystallized ligand in 5L42.

Conclusion

The chemical structure of thiadiazine thione, as dithiocarbamate has two separate portions; an amine part made by alkyl/aryl/aralkylamines or amino acids, which provoke the reactive oxygen species production. The second part, a carbon disulfide

end, that has the capability of chelation with metals, thus ascribing an important biological potential of this group of compounds against metalloproteases, which are key enzymes essential for parasitic biology. Due to the structural features of alkyl/aryl/aralkylamines or amino acids linked thiadiazine thiones, a number of pharmacological applications were examined in this scaffold. We successfully demonstrated bioactive potential of alkyl/aryl/aralkylamines or amino acids for the first time as antileishmanial and antibacterial agents. Compounds **4d** and **4f** exhibited potent antileishmanial activity which were further docked into the binding site of PTR1 where these molecules showed appropriate binding interactions and docking scores, suggesting that PTR1 could be their druggable target. Both the molecules showed good physicochemical/medicinal properties and drug-likeness in ADME analysis. Moreover, MD simulation of **4d** also indicates good binding potential of **4d** with PTR1. Moreover, compounds **7**, **5d** and **5e** showed significant inhibitory potential for *S. aureus* and all the compounds revealed significant inhibition of *K. pneumoniae*, indicating dual efficacy of compounds **5d**, **5e** and **7**. This early-stage study identifies lead scaffolds with dual antileishmanial and antibacterial activity, providing proof-of-concept for biological efficacy, with future SAR-guided optimization expected to enhance potency of compounds.

Experimental section

The chemicals used in this research are of analytical grade as they were purchased from standard chemical vendors. Glass capillaries were used to get the melting points, which are uncorrected. Thin layer chromatography with precoated silica gel plates (thickness 0.2 mm and 60 HF-254) was used to know the progress of synthesis. The Nuclear Magnetic Resonance Spectroscopy (NMR) analysis was recorded using a Bruker Avance 400 MHz spectrometer for both ^{1}H and ^{13}C observations, using DMSO-d^6, Methanol-d^4, and $CDCl_3$ as solvents. The downfield shifts were expressed in parts per million (ppm) using tetramethylsilane (TMS) as the reference standard. The Bruker Vector 22 FTIR Spectrometer was used for infrared spectroscopy. HRMS spectra were recorded on LC/MSD time-of-flight (TOF) spectrometer, using electrospray ionization (ESI) as the ionization method.

General procedure for the synthesis of THTTs (4a–i, 5a–g and 6)

The target thiadiazine thions were synthesized as previously described.[14] Conventional one pot domino synthesis was carried out (Scheme 1). The synthesis involved taking alkyl/cycloalkyl/aralkylamines or amino acids (20 mmol) in 30 mL basic water containing KOH (20%, 1120 mg). The reaction mixture was stirred for 15 minutes. In the next step, CS_2 (20 mmol, 2.4 mL) was added over 15 minutes and agitated for 4 h. To the resulting dithiocarbamate salt, which acted as reaction intermediate, two equivalent of formaldehyde (3.18 mL, 40 mmol) was added and subjected to cyclocondensation with amines (furfuryl amine and benzylamine) and amino acids (2-aminobutanoic acid, glycine) in a suspension of phosphate buffer (pH 7.8–8). After one hour stirring, the solution was filtered, followed by thrice extraction with DCM. Furthermore, the filtrate was chilled and acidified with 15% HCl. The precipitates obtained after acidification were cleaned with water and chilled methanol, dried and recrystallized to yield the final product.

Synthesis of 2-(5-methyl-6-thioxo-1,3,5-thiadiazinan-3-yl) butanoic acid (4a). White solid, m.p. 124–125 °C; yield: 77%; soluble in: methanol, DMSO, chloroform; IR: 2820 (C–H), 1510 (C=S) cm^{-1}, 1710 (C=O); ^{1}H NMR (methanol-d^4) δ 4.51–4.63 (m, 4H, H/4 and H/6), 3.57 (dd, 1H, J = 8 Hz, 4 Hz, CHCOOH), 3.40 (s, 3H, N-CH_3), 1.74–1.92 (m, 2H, CH_3CH_2CH), 0.93 (t, 3H, J = 8 Hz, CH_3CH_2CH); ^{13}C NMR (methanol-d^6): δ 192.2, 174.2, 68.5, 62.9, 56.4, 39.3, 22.8, 8.6; HRMS (ESI) m/z value calcd for $C_8H_{14}N_2O_2S_2$ $[M + H]^+$ 235.0569, found value: 235.0568.

Synthesis of 2-(5-ethyl-6-thioxo-1,3,5-thiadiazinan-3-yl) butanoic acid (4b). White solid, m.p. 127–129 °C; yield 62%; soluble in: DMSO, water; IR: 2938 (C–H), 1517 (C=S) 1706 (C=O) cm^{-1}; ^{1}HNMR (methanol-d^4, 400 MHz) δ 4.61 (dd, 2H, J = 12 Hz, 4 Hz, H/6), 4.43–4.52 (dd, 2H, J = 16 Hz, 12 Hz, H/4), 4.17–4.26 (m, 1H, CH_3CH_{2b}), 3.75–3.84 (m, 1H, CH_3CH_{2a}), 3.54 (m, 1H, m, dd, J = 8 Hz, 4 Hz, CHCOOH), 3.54 (dd, 1H, J = 8 Hz, 4 Hz, CHCOOH), 1.20 (t, 3H, J = 8 Hz, N-CH_2CH_3), 0.94 (t, 3H, J = 8 Hz, CH_3CH_2CH); ^{13}C NMR (Methanol-d^4): δ 191.6, 173.9, 67.3, 62.5, 55.3, 46.8, 22.6, 10.5, 8.39. HRMS (ESI) m/z value calcd for $C_9H_{16}N_2O_2S_2$ $[M + H]^+$ 249.07314, found value: 249.07314.

Synthesis of 2-(5-propyl-6-thioxo-1,3,5-thiadiazinan-3-yl) butanoic acid (4c). White solid, m.p. 101–102 °C; soluble in: methanol, DMSO; yield 72%; IR: 2956 (C–H), 3250 (COOH), 1730 (C=O), 1506 (C=S) cm^{-1}; ^{1}H NMR (methanol-d^4, 400 MHz) δ 4.59–4.63 (m, 4H, H/4, H/6), 4.40–4.53 (m, 1H, CH_3-CH_2CH_{2b}), 3.89–3.93 (m, 1H, $CH_3CH_2CH_{2a}$), 3.53–3.58 (m, 1H, CH_3CH_2CH), 1.81–1.91 (m, 2H, $CH_3CH_2CH_2$), 1.54–1.72 (m, 2H, CH_3CH_2CH), 1.00 (t, 3H, J = 4 Hz, $CH_3CH_2CH_2$), 0.92 (t, 3H, J = 8 Hz, CH_3CH_2CH), ^{13}C NMR (DMSO-d^6): δ 191.1, 174.0, 67.7, 62.3, 55.1, 52.3, 26.0, 22, 12.9, 8.38; HRMS (ESI) m/z value calcd for $C_{10}H_{18}N_2O_2S_2$ $[M + H]^+$ 263.0879, found value: 263.0882.

Synthesis of 2-(5-octyl-6-thioxo-1,3,5-thiadiazinan-3-yl) butanoic acid (4d). White solid, m.p. 139–134 °C; soluble in: methanol, DMSO and chloroform; yield 76%; IR: 3227 (COOH), 2925 (C–H), 1701(C=O), 1500 (C=S) cm^{-1}; ^{1}H NMR (DMSO-d^6) δ 4.55 (dd, 2H, J = 16 Hz, 8 Hz, H/4), 4.42 (dd, 2H, J = 20, 12 Hz, 12 Hz, H/6), 3.95–4.02 (m, 1H, NCH_{2b}), 3.63–3.70 (m, 1H, NCH_{2a}), 3.35 (dd, 1H, J = 8 Hz, 4 Hz), 1.65–1.79 (m, 2H, CH_2), 1.46–1.57 (m, 2H, CH_2), 1.20–1.25 (m, 10H), 0.790.83 (m, 6H, $2CH_3$), HRMS (ESI) m/z value calcd for $C_{15}H_{28}N_2O_2S_2$ $[M + H]^+$ 333.1665, found value: 333.1652.

Synthesis of 2-(5-dodecyl-6-thioxo-1,3,5-thiadiazinan-3-yl) butanoic acid (4e). White solid, m.p. 136–137 °C; soluble in: methanol, DMSO; yield 61; IR: 3428 (COOH), 1707 (C=O), 2923 (C–H), 1502 (C=S) cm^{-1}; ^{1}H NMR (methanol-d^4) δ 4.60 (dd, 2H, J = 12, 4 Hz, H/4), 4.46 (dd, 2H, J = 20, 16 Hz, H/6), 4.09–4.17 (m, 1H, NCH_{2b}), 3.67–3.77 (m, 1H, NCH_{2a}), 3.55 (dd, 1H, J = 8, 4 Hz, CHCOOH), 1.79–1.93 (m, 2H, $CH_2CHCOOH$), 1.59–1.71 (m, 2H, NCH_2CH_2), 1.27–1.32 (m, 18H, 9-CH_2's), 0.93 (t, 3H, J = 8,

CH_3CH_2CH), 0.87 (t, 3H, J = 8, dodecyl-CH_3), ^{13}C NMR (methanol-d^4): δ 191.0, 174.1, 67.8, 62.4, 55.3, 52.0, 22.6, 26.0, 26.3, 28.8, 29.0, 29.1, 29.2, 29.29, 29.3, 31.6, 22.2, 13.0, 8.39; HRMS (ESI) m/z value calcd for $C_{19}H_{36}N_2O_2S_2$ $[M + H]^+$ 389.2291, found value: 389.2286.

Synthesis of 2-(5-benzyl -6-thioxo-1,3,5-thiadiazinan-3-yl) butanoic acid (4f). White solid, m.p. 129–130 °C; soluble in: DMSO, methanol; yield 77%; IR: 2923 (C–H), 1500 (C═S), 3499 (COOH), 1703 (C═O) cm^{-1}; ^{1}H NMR (DMSO-d^6): δ 7.18–7.35 (m, 5H, Ar), 5.4 (d, 1H, J = 12 Hz, $ArCH_{2b}$), 5.01 (d, 1H, J = 16 Hz, $ArCH_{2a}$), 4.62 (d, 2H, J = 12), 4.41 (d, 2H, J = 12), 3.28 (t, 1H, J = 8 Hz, CHCOOH), 1.35–1.45 (m, 2H, CH_3CH_2), 0.63 (t, 3H, J = 8 Hz, CH_3CH_2); ^{13}C NMR (DMSO-d^6): δ 192.7, 172.8, 136.2, 129.0, 128.1, 128.5, 67.2, 62.3, 56.7, 53.6, 22.7, 9.68; HRMS (ESI) m/z value calcd for $C_{14}H_{18}N_2O_2S_2$ $[M + H]^+$ 311.0882, found value: 311.0874.

Synthesis of 2-(5-(furan-2-ylmethyl)-6-thioxo-1,3,5-thiadiazinan-3-yl)butanoic acid (4g). White solid, m.p. 126–127 °C; soluble in: methanol, DMSO, chloroform; yield 73%; IR: 1495 (C═S), 3431 (COOH), 1705 (C═O), 2915 (CH) cm^{-1}; ^{1}H NMR (methanol-d^4) δ 7.43 (dd, 1H, J = 4, H/11), 6.43 (d, 1H, J = 4 Hz, H/10), 6.3 (dd, 1H, J = 4 Hz, H-9), 5.27 (q, 2H, J = 24, 16 Hz, furfuryl-CH_2), 4.62 (s, 2H, H/4), 4.52 (s, 2H, H/6), 3.48 (dd, 1H, J = 8 Hz, 4 Hz (CHCOOH)), 1.62–1.74 (m, 2H, CH_3CH_2), 0.84 (t, 3H, J = 8, CH_3CH_2), ^{13}C NMR (methanol-d^4): δ 193.2, 173.9, 148.9, 142.4, 110.1, 109.7, 66.9, 62.0, 55.9, 46.3, 22.4, 8.1; HRMS (ESI) m/z value calcd for $C_{12}H_{16}N_2O_3S_2$ $[M + H]^+$ 301.0675, found value: 301.0673.

Synthesis of 2-(5-phenyl-6-thioxo-1,3,5-thiadiazinan-3-yl) butanoic acid (4h). White solid, m.p. 104–105 °C; soluble in: DMSO; chloroform; yield 64%; IR: 1465 (C═S), 1711 (C═O), 2981 (aliphatic C–H) cm^{-1}; ^{1}H NMR (DMSO-d^6, 400 MHz) δ 7.0–7.5 (m, 5H, Ar), 4.5–5.4 (m, 4H, H/4 and H/6), 3.59–3.62 (m, 1H, CHCOOH), 1.72–1.81 (m, 2H, CH_3CH_2), 0.80–0.86 (m, 3H, CH_3CH_2); HRMS (ESI) m/z value calcd for $C_{13}H_{16}N_2O_2S_2$ $[M + H]^+$ 297.0731, found value: 297.0725.

Synthesis of 2-(5-cyclohexyl-6-thioxo-1,3,5-thiadiazinan-3-yl) butanoic acid (4i). White solid; m.p. 132–133 °C; soluble in: chloroform, DMSO; yield 66%; IR: 3328 (COOH), 1595 (C═S), 2950 (C–H), 1720(C═O) cm^{-1}; ^{1}H NMR (DMSO-d^6, 300 MHz) δ 12.95 (s, 1H (broad), COOH), 5.60 (t, 1H, J = 12 Hz, CHCOOH), 4.32–4.61 (m, 4H, H/6, H/4), 3.37 (t, 1H, J = 6.9 Hz, NCH), 1.1–1.8 (m, 12H, cyclohexyl ring protons, CH_3CH_2), 0.8 (t, 3H, J = 12.3 Hz, CH_3CH_2), ^{13}C NMR (DMSO-d^6, 75 MHz) δ 190.82, 173.16, 63.54, 61.76, 58.30, 54.38, 28.80, 28.50, 25.82, 25.65, 25.18, 22.91, 9.79.

Synthesis of 2-(5-benzyl-2-thioxo-1,3,5-thiadiazinan-3-yl) butanoic acid (5a). White solid, m.p. 121–123 °C; soluble in: DMSO, chloroform; yield 57%; IR: 3405 (COOH), 1507 (C═S), 1707 (C═O), 2913 (aliphatic CH) cm^{-1}; ^{1}H NMR (DMSO-d^6): δ 7.23–7.32 (m, 5H, Ar), 4.50 (s, 2H, CCH_2N), 4.46 (d, 2H, J = 12, H/4), 4.25 (d, 2H, J = 12, H/6), 3.95 (q, 1H, J = 20,16 Hz, CHCOOH, 1.89–2.00 (m, 2H, CH_3CH_2)), 0.89 (t, 3H, J = 4 Hz, CH_3CH_2), ^{13}C NMR (DMSO-d^6): δ 192.7, 172.8, 136.2, 129.0, 128.5, 128.1, 67.2, 62.3, 56.7, 53.6, 22.7, 9.68; HRMS (ESI) m/z value calcd for $C_{14}H_{18}N_2O_2S_2$ $[M + H]^+$ 311.0882, found value: 311.0872.

Synthesis of 2-(5-(furan-2-ylmethyl)-2-thioxo-1,3,5-thiadiazinan-3-yl)butanoic acid (5b). Reddish solid, m.p. 119–120 °C; yield 55%; IR: 2975 (aliphatic C–H), 1495 (C═S), 1725 (C═O) cm^{-1}; ^{1}H NMR (DMSO-d^6) δ 7.59 (d, 1H, H-15), 6.36–6.69 (m, 2H, H/13, H/14), 4.52 (d, 2H, J = 12, H/4), 4.45 (s, 2H, CCH_2N), 4.24 (d, 2H, J = 12, H/6), 3.95 (t, 1H, J = 16, CHCOOH), 1.91–2.02 (m, 2H, CH_3CH_2), 0.88 (t, 3H, J = 8, CH_3CH_2); ^{13}C NMR (methanol-d^4): δ 193.2, 173.9, 148.9, 142.4, 110.1, 109.7, 66.9, 62.0, 55.9, 46.3, 22.4, 8.1; HRMS (ESI) m/z value calcd for $C_{12}H_{16}N_2O_3S_2$ $[M + H]^+$ 301.0675, found value: 301.0668.

Synthesis of 5-(furan-2-ylmethyl)-3-phenyl-1,3,5-thiadiazinane-2-thione (5c). Greenish crystals, m.p. 85–86 °C; soluble in: DMSO, chloroform; yield 57; IR: 1496 (C═S), 2910 (aliphatic C–H), 1500–1475 (C═C) cm^{-1}; ^{1}H NMR (DMSO-d^6) δ 7.59 (dd, 1H, J = 4 Hz, H-15), 7.20–7.44 (m, 5H, Ar), 6.43 (d, 1H, J = 4 Hz, H-14), 6.37 (dd, 1H, J = 4 Hz, H-13), 4.59 (s, 2H), 4.56 (s, 2H), 4.09 (s, 2H); ^{13}C NMR (DMSO-d^6): δ 193.3, 150.4, 144.8, 143.8, 129.9, 128.2, 127.6, 111.0, 110.4, 72.4, 58.0, 47.0; HRMS (ESI) m/z value calcd for $C_{14}H_{14}N_2OS_2$ $[M + H]^+$ 291.062, found value: 291.061.

Synthesis of 2-(5-(2-hydroxyethyl)-6-thioxo-1,3,5-thiadiazinan-3-yl)acetic acid (5d). Yellowish solid; m.p. 133–135 °C; soluble in: DMSO, chloroform; yield 60%; IR: 2910 (C–H), 1503 (C═S), 3370 (OH), 1706 (C═O) cm^{-1}; ^{1}H NMR (DMSO-d^6) δ 5.53 (s, 2H, H/4), 4.47 (s, 2H, H/6), 3.94 (t, 2H, J = 4 Hz, $HOCH_2$), 3.60 (t, 2H, J = 4 Hz,CH_2CH_2N), 3.52 (s, 2H, CH_2-COOH); ^{13}C NMR (DMSO-d^6): δ 191.0, 171.0, 72.0, 58.6, 58.5, 54.5, 51.2; HRMS (ESI) m/z value calcd for $C_7H_{12}N_2O_3S_2$ $[M + H]^+$ 237.0362, found value: 237.0358.

Synthesis of 3-methyl-5-(pyridin-4-yl)-1,3,5-thiadiazinane-2-thione (5e). White solid; m.p. 90–91 °C; soluble in: chloroform, methanol; yield 58%; IR: 3030 (Ar CH), 1605 (C═N), 2882 (aliphatic C–H), 1540 (C═S) cm^{-1}; ^{1}H NMR (DMSO-d^6) δ 8.05 (d, 2H, J = 8 Hz, H-10), 6.59 (d, 2H, J = 4, H-9), 4.48 (d, 4H, J = 8, H-6, H-4), 3.73 (s, 3H, CH_3N).

Synthesis of 2-(5-cyclohexyl-2-thioxo-1,3,5-thiadiazinan-3-yl) butanoic acid (5f). White solid; m.p. 121–122 °C; soluble in: chloroform, DMSO; yield 65%; IR: 3427 (COOH), 1731 (C═O), 2935 (C–H), 1499 (C═S) cm^{-1}; ^{1}H NMR (DMSO-d^6) δ 5.61–5.68 (m, 1H, NCHCOOH), 4.52 (d, 4H, J = 12 Hz, H/6, H/4), 2.58–2.59 (m, 1H, NCH), 1.09–1.93 (m, 12H, cyclohexyl protons and CH_3CH_2), 1–1.4 (m, 3H, CH_3CH_2); ^{13}C NMR (DMSO-d^6) δ 191.22, 173.16, 62.67, 62.01, 55.34, 54.20, 30.76, 28.50, 25.83, 25.74, 25.05, 24.89.

Synthesis of 3,5-diisopropyl-1,3,5-thiadiazinane-2-thione (5g). White solid; m.p. 123–124 °C; soluble in: chloroform, DMSO; yield 57%; ^{1}H NMR (DMSO-d^6) δ 5.95–6.04 (m, 1H, ^{3}NCH), 4.55 (d, 2H, J = 4.6 Hz, H/4), 4.49 (d, 2H, J = 3.6 Hz, H/6), 2.89–2.98 (m, 1H, ^{5}NCH), 1.172 (d, 6H, J = 7.2, $(CH_3)_2CHN_3$), 1.139 (d, 6H, J = 6.3 Hz $(CH_3)_2CHN^5$), ^{13}C NMR (DMSO-d^6) δ 190.91, 62.01, 54.77, 50.0, 47.65, 21.35, 18.61.

Synthesis of (5-butyl-6-thioxo-1,3,5-thiadiazinan-3-yl)acetic acid (6). White solid; m.p. 145–146 °C; soluble in: ethanol; yield (79%); IR ν max: 3201 (COOH), 1735(C═O), 2869 (C–H), 1506 (C═S); ^{1}H NMR (CD_3OD) δ 4.53 (s, 2H, H/4), 4.52 (s, 2H, H/6), 3.97 (t, 2H, J = 8.0 Hz, CH_2CH_2N), 3.63 (s, 2H, CH_2CO), 1.61–

1.67 (m, 2H, $CH_3CH_2CH_2$), 1.32–1.39 (m, 2H, CH_3CH_2), 0.96 (t, 3H, J = 7.2 Hz, CH_3CH_2).[25]

Synthesis of methyl 2-(5-butyl-6-thioxo-1,3,5-thiadiazinan-3-yl)butanoate: an ester analogue (7). Over ten minutes, $SOCl_2$ (1.50 mmol, 0.1 mL) was added to a continuously stirred mixture of compound **6** (1 mmol, 2480 mg) in 10 mL of cooled methanol. After stirring for 35 minutes, 25 mL of cooled water was added to the flask. For the ester analogue extraction, ethyl acetate was utilized, while calcium chloride was used for drying and a 10% saturated sodium bicarbonate solution for washing. Upon rotary evaporation of ethyl acetate gave ester as colorless crystals; yield 59%, m.p. 75 °C; soluble in: chloroform, ethyl acetate; IR: 2913 (C–H), 1745 (C=O), 1510 (C=S) cm^{-1}; 1H NMR (DMSO-d^6) δ 4.46 (d, 4H, J = 8, H/4 and H/6), 3.85 (t, 2H, J = 8 Hz, CH_2CH_2N), 3.61 (s, 3H, OCH_3), 3.58 (s, 2H, CH_2CO), 1.46–1.54 (m, 2H, J = 8 Hz, 4 Hz,$CH_3CH_2CH_2$), 1.18–1.27 (m, 2H, J = 8 Hz, 4 Hz, CH_3CH_2), 0.82 (t, 3H, J = 4 Hz, CH_3CH_2); ^{13}C NMR (DMSO-d^6): δ 190.3, 170.1, 69.9, 58.4, 52.2, 51.3, 51.2, 28.3, 19.9, 14.1; HRMS (ESI) m/z value calcd for $C_{10}H_{18}N_2O_2S_2$ $[M + H]^+$ 263.0882, found value: 263.08.

Biological activities

Antileishmanial assay. Antileishmanial activity of the synthesized analogues was examined using published method with slight modification.[30] A pre-established culture of *Leishmania tropica* was maintained in RPMI-1640 medium and incubated at 24 °C for 6–7 days. Stock solutions (1000 μg mL^{-1}) of each compound were prepared by dissolving 1 mg of the respective compound in 1 mL of DMSO. These stock solutions were further serially diluted. In separate 96-well microtiter plates, 180 μL of 199 medium was dispensed into each well. Twenty microliters of each test sample were added to the first well and serially diluted across the plate. To maintain a final volume of 180 μL per well, 20 μL was removed from the last well after dilution. Subsequently, 100 μL of the parasite suspension was added to each well. Two rows were designated for controls: DMSO as the negative control and amphotericin B as the positive control, both serially diluted with RPMI-1640 medium. The plates were incubated in a shaker incubator at 24 °C for 72 hours. All assays were performed in triplicate. Following incubation, 20 μL from each well was transferred to an improved Neubauer counting chamber to quantify live parasites. The percentage inhibition for each compound was calculated, and IC_{50} values for compounds exhibiting antileishmanial activity were determined using GraphPad Prism software.

Antibacterial assay. The antibacterial potential of the synthesized compounds was evaluated using the agar well diffusion method. Clinical isolates of *Staphylococcus aureus* and *Klebsiella pneumoniae* were obtained from Khyber Medical University. Müller–Hinton Broth (MHB) was prepared by dissolving 2 g of MHB powder in 100 mL of distilled water, adjusting the pH to 7.0, and autoclaving. Müller–Hinton Agar (MHA) was prepared by dissolving 3.8 g of MHA in 100 mL of distilled water, adjusting the pH to 7.0, and autoclaving at 121 °C. The sterilized MHA was poured into sterile Petri plates. A 0.5 McFarland standard, corresponding to ~1.5×10^8 CFU mL^{-1}, was prepared by mixing 0.05 mL of 1.175% barium chloride dihydrate ($BaCl_2 \cdot 2H_2O$) with 9.95 mL of 1% sulfuric acid (H_2SO_4). Bacteria were cultured in MHB overnight prior to the assay, and the inoculum density was adjusted to match the 0.5 McFarland standard. The standardized bacterial suspension was spread evenly on the surface of the MHA plates. Wells of 4 mm diameter were aseptically bored into the agar, and the test compounds were introduced into individual wells. Plates were incubated at 37 °C for 24 hours. Zones of inhibition were measured in millimeters (mm), and results were recorded and interpreted accordingly.

Molecular docking and ADME analysis of 4d and 4f. The three-dimensional structure of PTR1 was retrieved from Protein data bank (5L42) for docking of two most active antileishmanial compounds **4d** and **4f**. Molecular Operating Environment (MOE 2022.02) was employed to analyze the binding affinity of our inhibitors with PTR1. The compounds structures were drawn on MOE and minimized at 0.50 RMS gradient with MMFF-94x force field after applying AM1-BCC charges. The PTR1 structure (5L42) is complexed with an inhibitor ((2~{*R*})-2-[3,4-bis(oxidanyl)phenyl]-6-oxidanyl-2,3-dihydrochromen-4-one) which interacts with the coenzyme in the complex. This ligand was used as a standard inhibitor in docking. The missing bonds and atoms in the protein structure were fixed by MOE Loop builder tool and Quick Prep Module using the Amber14: EHT force field. We initially scrutinized the docking protocol of MOE (which is triangle matcher by default with London dG) by re-docking of complex ligand in 5L42. Re-docking showed good results with a RMSD of 0.17 Å (Fig. 6) and docking score of −5.88 kcal mol^{-1} for co-crystallized ligand. Because of good re-docking results, we used the same docking protocol to dock **4d** and **4f** with conformations set to 100. The docking results were analyzed in MOE interface.

The physicochemical (ADME: absorption, distribution, metabolism, and excretion) and drug-like properties of **4d** and **4f** were predicted by SwissDME server (**http://www.swissadme.ch**) by providing their SMILE strings (**4d**: CCCCCCCCN1CN(CSC1=S)C(C(=O)O)CC, **4f**: CCC(C (=O)O) N1CSC(=S)N(C1)Cc1ccccc1) to the server.

Molecular dynamics (MD) simulations. Compound **4d** is the best inhibitor in the *in vitro* and the docking studies, therefore, standard inhibitor (STD) and **4d** (in complex with PTR1) were subjected to the molecular dynamics simulations for 200 ns. The simulation was conducted in the cubic box with dimensions of 8.97 Å and 8.76 Å with water molecules of 20 829 and 20 679, respectively for STD and **4d**. Moreover, single sodium ion was added to neutralized both systems and SPC216 model was used to solvate these systems.[31,32] GROMACS version 2022.06 was used in MD simulation.[33] Generalized Amber Force Field (GAFF) was applied for cofactor NADP, STD and **4d** parameterization, while the protein was parametrized by Amber99SB force field implemented in AmberTools.[34] Post solvation steepest-descent algorithm was implemented for energy minimization of 50 000 steps to remove all the poor interactions.[32] 0.5 ps with a 2 fs time difference was used for *NVT* equilibration by canonical ensemble. The modified Berendsen thermostat was used to slowly increase the temperature from 0 to 300 K over 0.5

ps of time constant.[35] Post *NVT*, the *NPT* equilibration of 0.5 ps by time step of 2 fs by isothermal-isobaric ensemble and the temperature was fixed at 300 K.[36] The pressure was fixed at 1.0 bar with the coupling time of barostat being 2 fs, implemented through the Parrinello–Rahman isotropic coupling method. After *NPT* equilibration, these systems were subjected to a simulation of 200 ns applied with a time variation of 2 fs. Applying isothermal compressibility of 4.5×10^{-5} bar^{-1}, the pressure and temperature were fixed at 1 bar and 300 K during simulation.[37] The LINCS algorithm was applied to constrain all hydrogen bonds. Long-range electrostatic interactions were treated by using Particle Mesh Ewald (PME) summation approach through 0.16 nm of fourier spacing with 4 order.[37] The electrostatic short-range contact and cutoff radii of van der Waals were set up to 1 nm. The structural and dynamical structures were computed with a 2 picosecond time difference throughout all trajectories.

Author contributions

Rasool Khan: conceptualization, methodology, data curation, writing—original draft. Sumaya Raheem: methodology, data curation, writing—original draft. Sobia Ahsan Halim: methodology, formal analysis, writing—review & editing. Midrar Ullah: methodology, data curation, writing—original draft. Haleema Ali: software, data curation, formal analysis, Imdad Ullah Khan: data curation, formal analysis, investigation. Momin Khan: methodology, investigation, formal analysis. Hanan A. Ogaly: formal analysis, resources, funding acquisition. Mohammad Zubair: data curation, investigation, methodology. Mesaik M. Ahmed: formal analysis, resources, writing—review & editing. Ajmal Khan: data curation, formal analysis, resources, writing—review & editing. Ahmed Al Harrasi: conceptualization, project administration, supervision, writing—review & editing.

Conflicts of interest

There is no conflict of interest.

Data availability

The data supporting this article have been included as part of the supplementary information (SI). Supplementary information (SI) is available. See DOI: **https://doi.org/10.1039/d5ra05994a**.

Acknowledgements

The authors extend their appreciation to the Deanship of Research and Graduate Studies at King Khalid University for funding this work through Large Research Project under grant number RGP2/95/46.

References

1 Y. M. Al-Kahraman, H. M. Madkour, D. Ali and M. Yasinzai, *Molecules*, 2010, **15**, 660–671.
2 C. R. Davies, P. Kaye, S. L. Croft and S. Sundar, *Bmj*, 2003, **326**, 377–382.
3 R. Reithinger, J.-C. Dujardin, H. Louzir, C. Pirmez, B. Alexander and S. Brooker, *Lancet Infect. Dis.*, 2007, **7**, 581–596.
4 Z. Dardari, M. Lemrani, A. Sebban, A. Bahloul, M. Hassar, S. Kitane, M. Berrada and M. Boudouma, *Arch. Pharmazie*, 2006, **339**, 291–298.
5 A. K. Shukla, B. K. Singh, S. Patra and V. K. Dubey, *Biotechnol. Appl. Biochem.*, 2010, **160**, 2208–2218.
6 A. B. Ozçelik, S. Ersan, A. U. Ural, S. Ozkan and M. Ertan, *Arzneim. Forsch.*, 2007, **57**, 554–559.
7 M. A. Hussein and M. Hashem, *Arch. Pharmazie*, 2008, **341**, 370–376.
8 A. N. El-Shorbagi, *Arch. Pharmazie*, 2000, **333**, 281–286.
9 H. Rodríguez, M. Suárez and F. Albericio, *Molecules*, 2012, **17**, 7612–7628.
10 A.-N. El-Shorbagi, H. Tarazi, M. Semreen and A. Hayallaha, *Int. J. Pharma Sci. Res.*, 2014, **5**, 460–469.
11 A.-N. El-Shorbagi, M. El-Naggar, H. Tarazi, S. Chaudhary, H. Abdu-Allah, F. Hersi and H. Omar, *Med. Chem. Res.*, 2018, **27**, 1103–1110.
12 A. A. Radwan, A. Al-Dhfyan, M. K. Abdel-Hamid, A. A. Al-Badr and T. Aboul-Fadl, *Arch Pharm. Res.*, 2012, **35**, 35–49.
13 A. Radwan, T. Aboul-Fadl, A. Al-Dhfyan and W. Abdel-Mageeda, *Asian J. Chem.*, 2014, **26**, 8145.
14 S. Raheem, R. Khan, X. Pan, R. Ullah, S. A. Halim, A. Khan and A. Al-Harrasi, *Bioorg. Chem.*, 2022, **127**, 105974.
15 J. Coro, R. Pérez, H. Rodríguez, M. Suárez, C. Vega, M. Rolón, D. Montero, J. J. Nogal and A. Gómez-Barrio, *Bioorg. Med. Chem.*, 2005, **13**, 3413–3421.
16 M. Ertan, S. Sarac and N. Yulug, *Arzneim. Forsch.*, 1990, **40**, 790–795.
17 M. Ertan, A. B. Tayhan and N. Yulug, *Arch. Pharmazie*, 1990, **323**, 605–609.
18 S. Saraç, M. Ertan, A. Balkan and N. Yulug, *Arch. Pharmazie*, 1991, **324**, 449–453.
19 X. Wang, X. Fu, J. Yan, A. Wang, M. Wang, M. Chen, C. Yang and Y. Song, *Mol. Diversity*, 2019, **23**, 573–583.
20 L. Monzote, A. M. Montalvo, L. Fonseca, R. Pérez, M. Suárez and H. Rodríguez, *Arzneimittelforschung*, 2005, **55**, 232–238.
21 N. Arshad, J. Hashim, M. A. Minhas, J. Aslam, T. Ashraf, S. Z. Hamid, T. Iqbal and S. Javed, *Bioorg. Med. Chem. Lett*, 2018, **28**, 3251–3254.
22 D. Molero, J. Coro, R. Pérez, M. Suárez, R. Martínez-Álvarez, A. Herrera and N. Martín, *Magn. Reson. Chem.*, 2007, **45**, 93–98.
23 J. N. Sangshetti, R. I. Shaikh, F. A. K. Khan, R. H. Patil, S. D. Marathe, W. N. Gade and D. B. Shinde, *Bioorg. Med. Chem. Lett*, 2014, **24**, 1605–1610.
24 D. Katiyar, V. Tiwari, R. Tripathi, A. Srivastava, V. Chaturvedi, R. Srivastava and B. Srivastava, *Bioorg. Med. Chem.*, 2003, **11**, 4369–4375.
25 V. Dufour, M. Stahl and C. Baysse, *Microbiology*, 2015, **161**, 229–243.
26 X. Li, M. Ni, X. Xu and W. Chen, *J. Enzyme Inhib. Med. Chem.*, 2020, **35**, 1773–1780.
27 W. M. Scheld, *Goldman's Cecil Medicine*, 2012, p. 1761.

28 E. Klein, D. L. Smith and R. Laxminarayan, *Emerg. Infect. Dis.*, 2007, **13**, 1840.
29 R. N. Jones, *Chest*, 2001, **119**, 397S–404S.
30 I. Khan, K. Ahmad, A. T. Khalil, J. Khan, Y. A. Khan, M. S. Saqib, M. N. Umar and H. Ahmad, *J. Tradit. Chin. Med.*, 2015, **35**, 316–322.
31 T. Makarewicz and R. Kazmierkiewicz, *J. Chem. Inf. Model.*, 2013, **53**, 1229–1234.
32 M. J. Abraham and J. E. Gready, *J. Comput. Chem.*, 2011, **32**, 2031–2040.
33 D. Boczar and K. Michalska, *Int. J. Mol. Sci.*, 2023, **24**, 16644.
34 P. Bhadra and S. W. Siu, *Langmuir*, 2019, **35**, 9622–9633.
35 S. Samantray, W. Schumann, A.-M. Illig, M. Carballo-Pacheco, A. Paul, B. Barz and B. Strodel, in *Computer Simulations of Aggregation of Proteins and Peptides*, Springer, 2022, pp. 235–279.
36 R. Hafner, G. Guevara-Carrion, J. Vrabec and P. Klein, *J. Phys. Chem. B*, 2022, **126**, 10172–10184.
37 M. Fernández-Pendás, B. Escribano, T. Radivojević and E. Akhmatskaya, *J. Mol. Model.*, 2014, **20**, 2487.